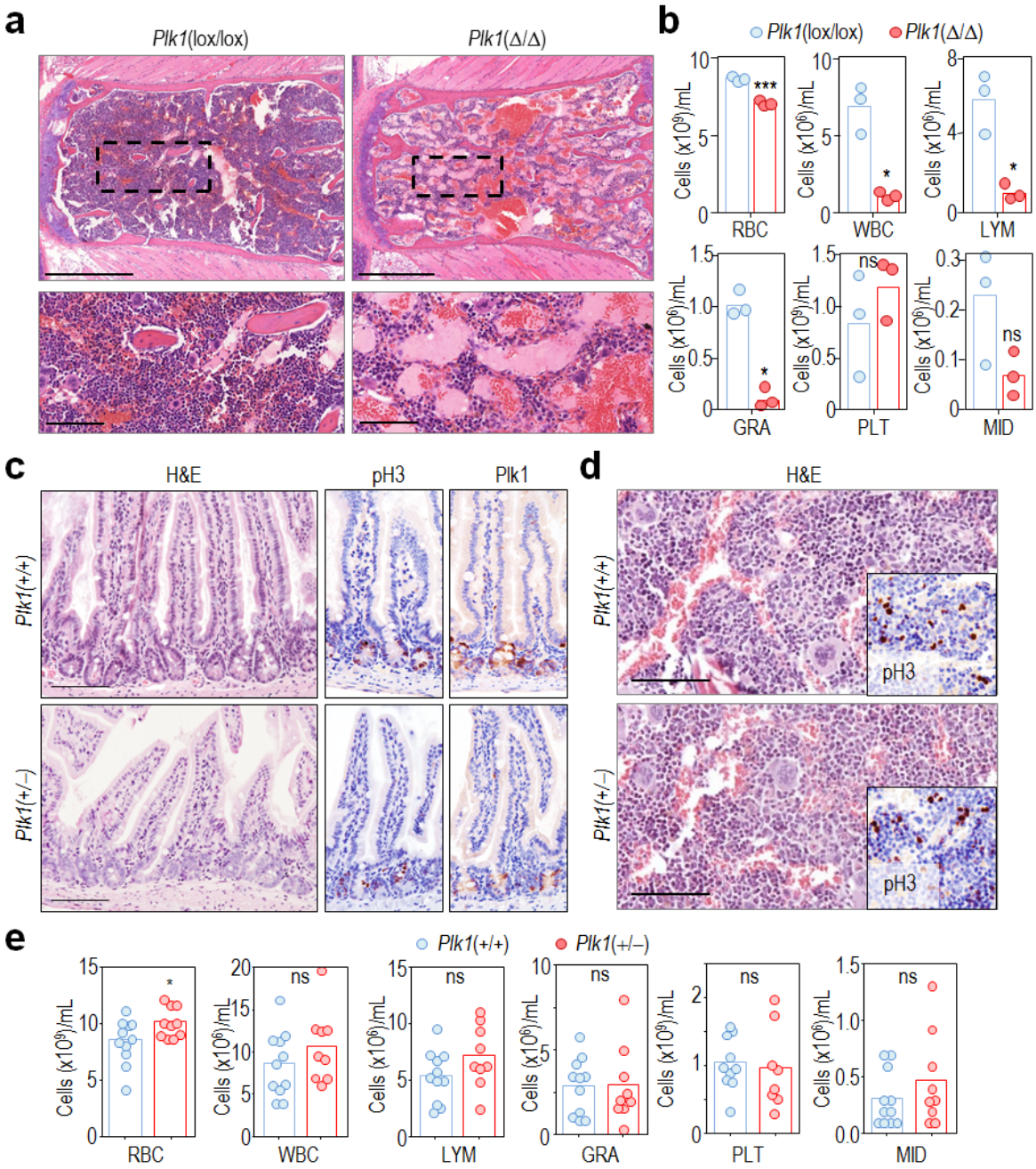

Supplementary Figure 1. Bone marrow and blood defects in Plk1-deficient mice. (a) Hypoplasia of the bone marrow [H&E staining; Scale bars 500 μm (upper panels) or 100 μm (lower panels)]. Micrographs are representative of 3 mice analyzed per genotype. (b) Defective blood cell populations after treatment with tamoxifen, including red (RBC) and white (WBC) blood cells, lymphocytes (LYM), and granulocytes (GRA). No significant differences were observed in platelets (PLT) or the mid-size group (MID) that includes monocytes, eosinophils and basophils seven days after tamoxifen injections. (c) Normal histology in the intestinal mucosa in Plk1-heterozygous mice. (d) Normal histology in bone marrow of Plk1-heterozygous mice. In (c, d) no differences are found in the percentage of phospho-histone H3 (pH3)-positive cells. (e) Peripheral blood cell populations in Plk1-heterozygous mice. The reason for the increased level of RBC is not known. In (b) and (e) columns indicate mean. ns, not significant; *, $p<0.05$; ***, $p<0.001$. Student's t-test.

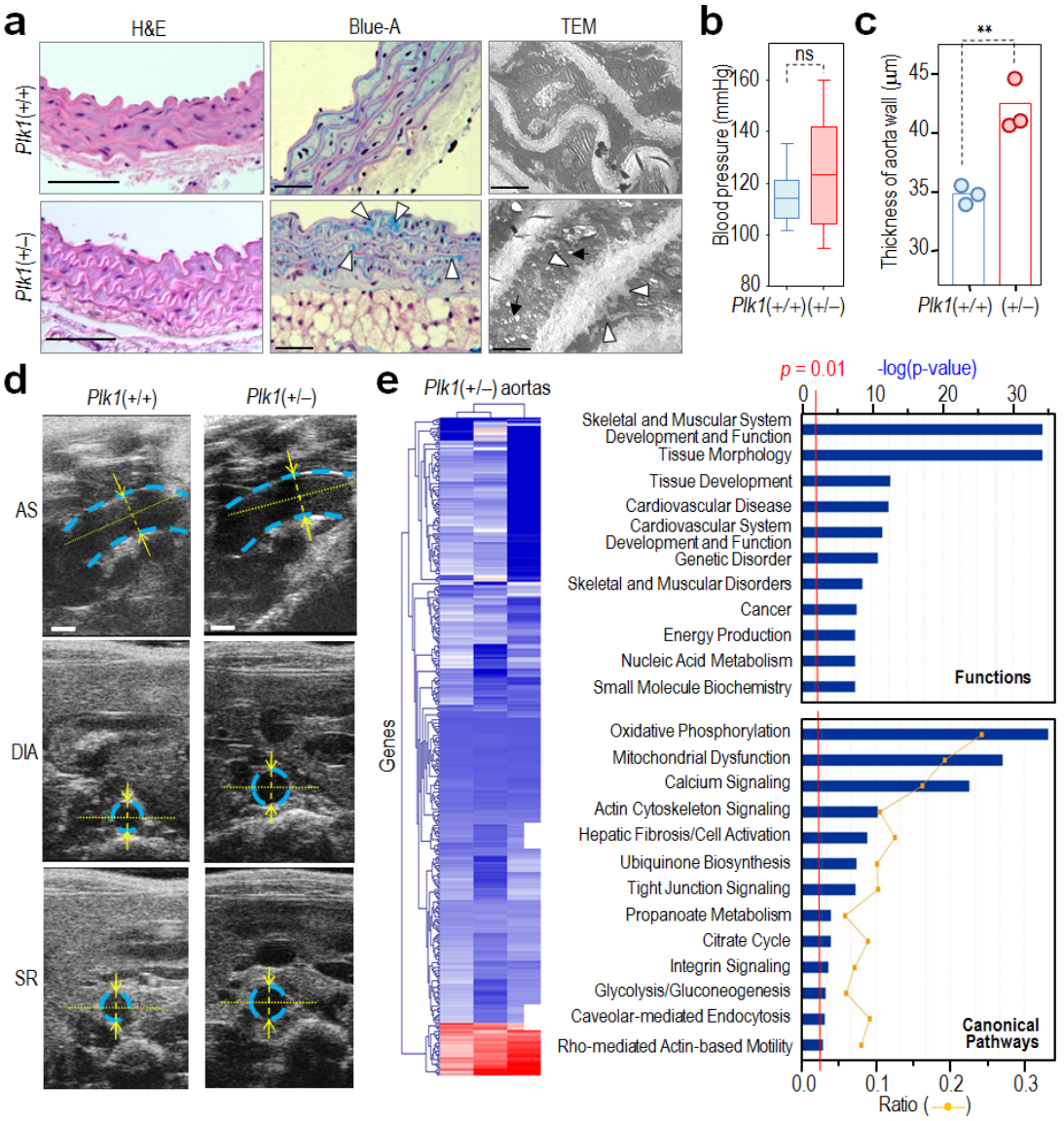

Supplementary Figure 2. Vascular defects in Plk1 heterozygous mice. (a) Aorta wall of *Plk1*(+/–) animals is thicker than wild type litter mates (left panels, H&E). These enlarged aortas show accumulation of mucopolysaccharides between elastic fibers as depicted by Alcian Blue staining (Blue-A; arrow heads), reflecting loss of elasticity. Transmission electron microscopy (TEM) panels show the fine ultra-structure of the aortic elastic fibers, with frequent disruption (open triangles) and vacuoles (arrows) in *Plk1*(+/–) mice. Scale bars, 100 μm (left), 50 μm (middle) and 10 μm (right panel). Micrographs are representative of 4 mice analyzed per genotype. (b) Blood pressure in mice with the indicated genotype. n=7 *Plk1*(+/+) and n=5 *Plk1*(+/–) mice. ns, not significant; Student's t-test. (c) Quantification of the aorta wall thickness (n=6 sections per animal; 3 mice per genotype). Columns indicate mean. **, p<0.01; Student's t-test. (d) Representative ultrasound images of three different segments of the mouse aorta (AS, ascending; DIA, diaphragmatic abdominal and SR, suprarenal abdominal sections) used to measure the maximal internal lumen width. Images are representative of 7 *Plk1*(+/+) and 5 *Plk1*(+/–) mice analyzed per genotype. Scale bars, 1 mm. (e) Transcriptional profiling in *Plk1*(+/–) and *Plk1*(+/+) aortas. Genes downregulated in *Plk1*(+/–) aortas are shown in blue whereas upregulated genes are in red. Each column represents the data from a *Plk1*(+/–) aorta compared to the pool of wild-type aortas. The functions and canonical pathways significantly deregulated in *Plk1*(+/–) aortas are indicated in the histograms. Columns show the –log(p-value) and the vertical red line indicates cutoff used (p=0.01; Fisher's exact test right-tailed). The ratio (number of genes in a given pathway that meet the cutoff criteria, divided by the total number of genes that make up that pathway in the reference gene set.) of these canonical pathways is shown with a yellow line (Ingenuity Pathway Analysis).

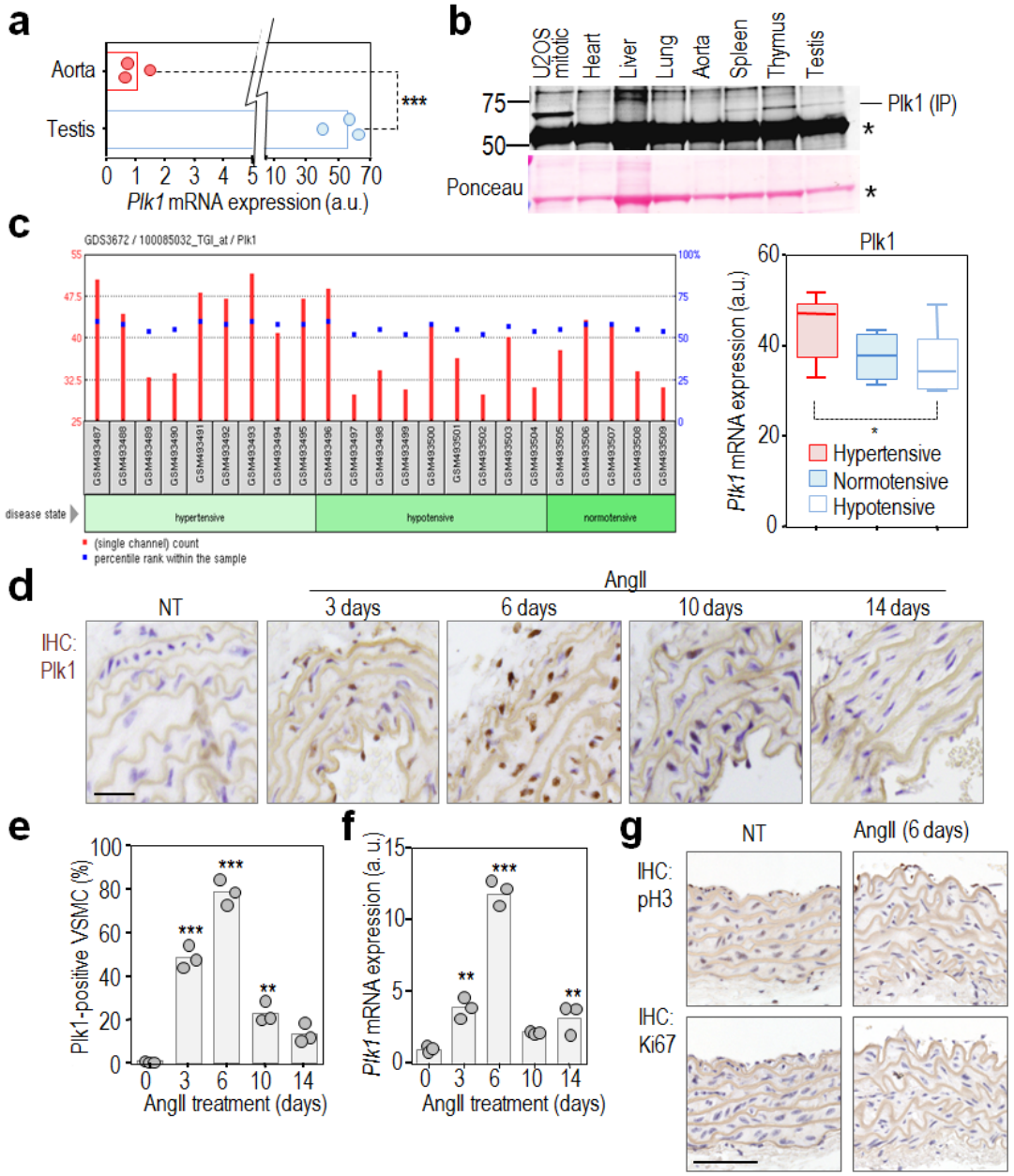

Supplementary Figure 3. Expression of Plk1 in murine aortas. (a) Plk1 mRNA (by qRT-PCR) expression analysis in the mouse aorta compared to mouse testis. Columns indicate mean; n=3 mice per genotype; ***, p<0.001; Student t-test. (b) Plk1 levels in proliferating tissues such as testis, and non-proliferating tissues such as heart, lung or aortas. Plk1 (was detected after immunoprecipitation with specific antibodies. Asterisks depict the IgG heavy chain of the immunoprecipitation antibody. (c) Quantification of the Plk1 expression data obtained from the GDS3672 GEO dataset (http://www.ncbi.nlm.nih.gov/sites/GDSbrowser?acc=GDS3672). Plk1 is significantly overexpressed in aortas from hypertensive animals when compared to hypotensive strains. Data indicate mean ± SEM; *,p<0.05 One-Way Anova test with Bonferroni's multiple comparison test. (d) Immunodetection of Plk1 (brown signal) in aortas at the indicated days after treatment with Angiotensin II (AngII). NT, not treated. Scale bars, 20 μm. (e) Percentage (n=500 cells) of VSMCs positive for Plk1 staining in aortas. (f) Quantification of Plk1 transcript levels by qRT-PCR in the same aortas from previous panels. In (e,f), columns indicate mean; n=3 mice per timepoint; *, p<0.05; **, p<0.01; ***, p<0.001; One-Way Anova test. (g) Descending aortas are negative for cell proliferation markers such as Ki67 or phospho-histone H3 (pH3) 6 days after treatment with AngII. Scale bars, 100 μm. Data in (d,g) are representative of sections from 3 mice per condition.

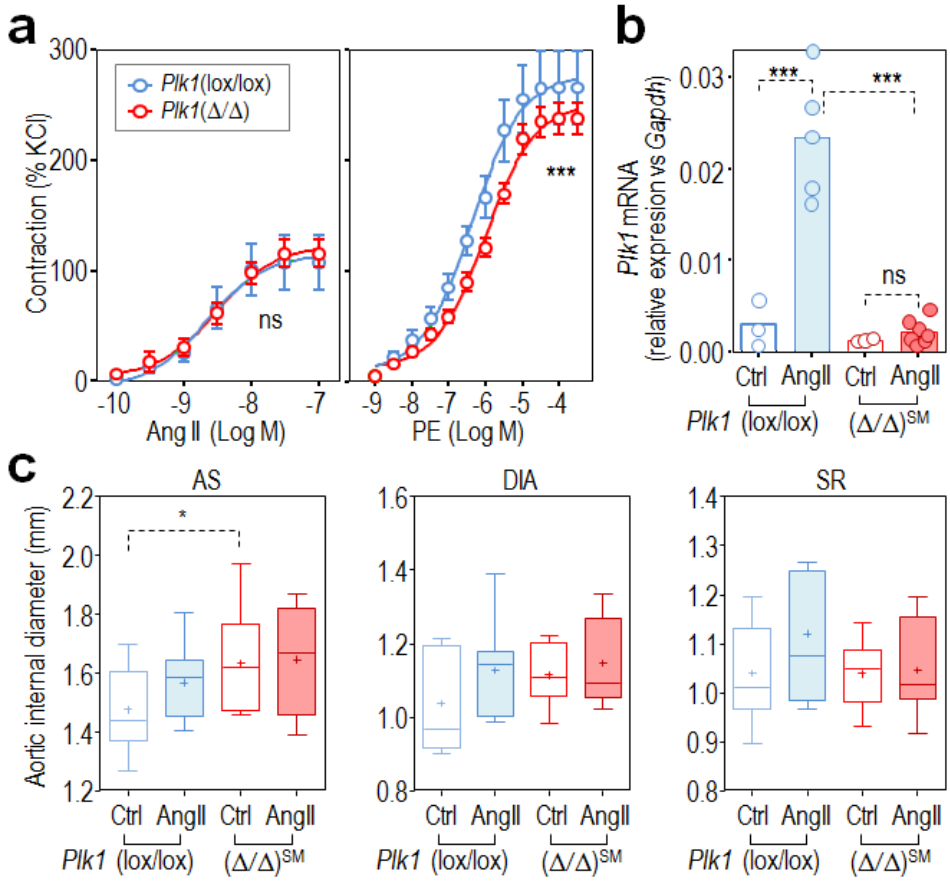

Supplementary Figure 4. Genetic ablation of Plk1 in VSMCs results in vascular defects. (a) Ex-vivo contraction test in rings from mesenteric arteries from mice with the indicated genotypes, in the presence of AngII or Phenylephrine (PE) at the indicated concentrations. Contraction is expressed as a percentage of the maximal KCl-induced contraction. Data are mean ± SEM from 4 thoracic rings per mouse (n=4 mice per condition). ns, not significant; ***, p<0.0001; Extra sum-of-squares F test. (b) *Plk1* mRNA levels (relative to *Gapdh* mRNA levels) in the aortas from *Plk1*(lox/lox) and *Plk1*(Δ/Δ)^{SM} mice 4 weeks after treatment with AngII or vehicle (Ctrl). Columns indicate mean; One-Way Anova. (c) Internal diameter of the ascending (AS), diaphragmatic (DIA) and suprarenal (SR) aortic in mice from Fig. 2g treated with AngII [*Plk1*(lox/lox) n=7; *Plk1*(Δ/Δ)^{SM} n=8] or untreated [Ctrl; *Plk1*(lox/lox) n=9; *Plk1*(Δ/Δ)^{SM} n=10] at the end of the experiment. *, p<0.05; Student's t-test.

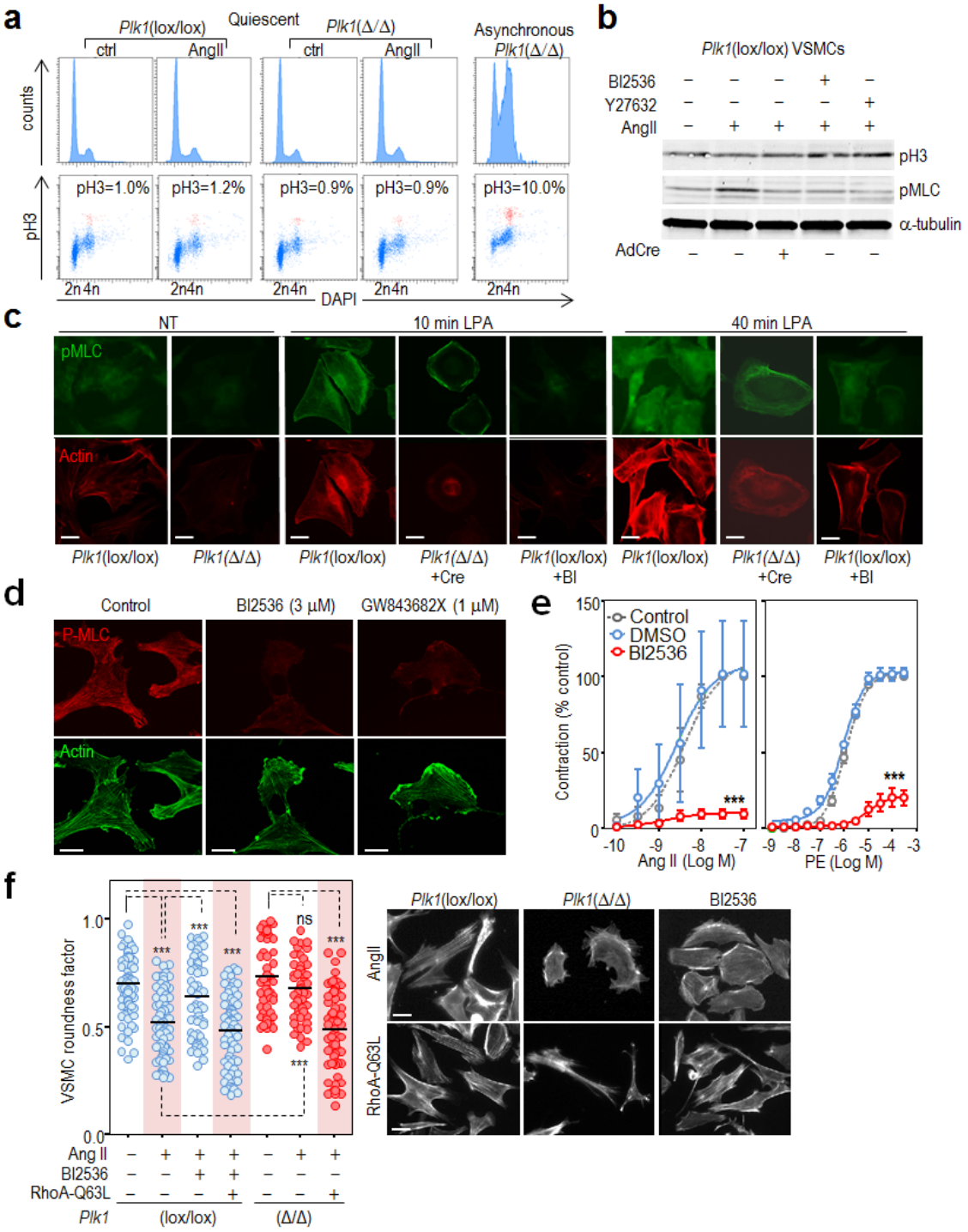

Supplementary Figure 5. Altered myosin dynamics and cell morphology in Plk1-deficient VSMCs. (a) DNA content analysis of *Plk1*(lox/lox) and *Plk1*(Δ/Δ) VSMCs. Cells were arrested by high confluency and serum starvation, and infected with AdenoCre viral particles. 48h after infection, cells were treated with 0.5 μM AngII and analyzed by FACS. The percentage of mitotic (phospho-Histone H3 Ser10-positive; pH3, red dots) cells is shown. Asynchronous VSMCs were infected with AdenoCre as a positive control for mitotic aberrations. (b) Control VMSCs were treated either with Plk1 (BI2536) or ROCK (Y27632) inhibitors or AdenoCre in the presence or absence of AngII or AdenoCre. These lysates were evaluated using phospho-Histone H3 (Ser10; pH3) or phospho-MLC(Ser18/19)-specific antibodies. α-tubulin was used as a loading control. (c) Plk1 depletion or inhibition in VSMCs inhibits the phosphorylation of the Myosin light chain protein (pMLC) upon LPA treatment. Plk1 depleted or inhibited (BI2536) VSMCs were stained with phospho Ser19-MLC antibody (green) and with Alexa594-phalloidin (red) after 10 and 40

minutes treatment with 2 μM LPA. Scale bars, 20 μm. (**d**) Immunofluorescence in VSMCs showing that kinase activity inhibition of Plk1 by chemical compounds (BI2536 and GW843682X) leads a reduction in the levels of phospho-MLC (Ser19) (red color) and less actin stress fibers (green color). Scale bars, 20 μm. (**e**) Ex-vivo contraction test in mesenteric artery rings in the presence of increasing concentrations of AngII or Phenylephrine (PE), and the Plk1 inhibitor BI2536 (red), DMSO as solvent (blue) or untreated samples (grey dashed). Contraction is expressed as a percentage of the maximal KCl-induced contraction in the untreated samples. Data are mean ± SEM from n=3 mice in the AngII set, and n=4 mice in the PE set. ns, not significant; ***, $p<0.0001$; Extra sum-of-squares F test. (**f**) Cell roundness in VSMCs in the absence or presence of Angiotensin II (AngII), Plk1 inhibitor (BI2536), or a constitutive version of RhoA (RhoA-Q63L). Roundness was calculated by using ImageJ software, and more than 50 cells were analyzed in each group. Bars indicate mean. ns, not significant; ***, $p<0.001$; One-Way Anova analysis. Representative images are shown in the right panels, Scale bars, 20 μm.

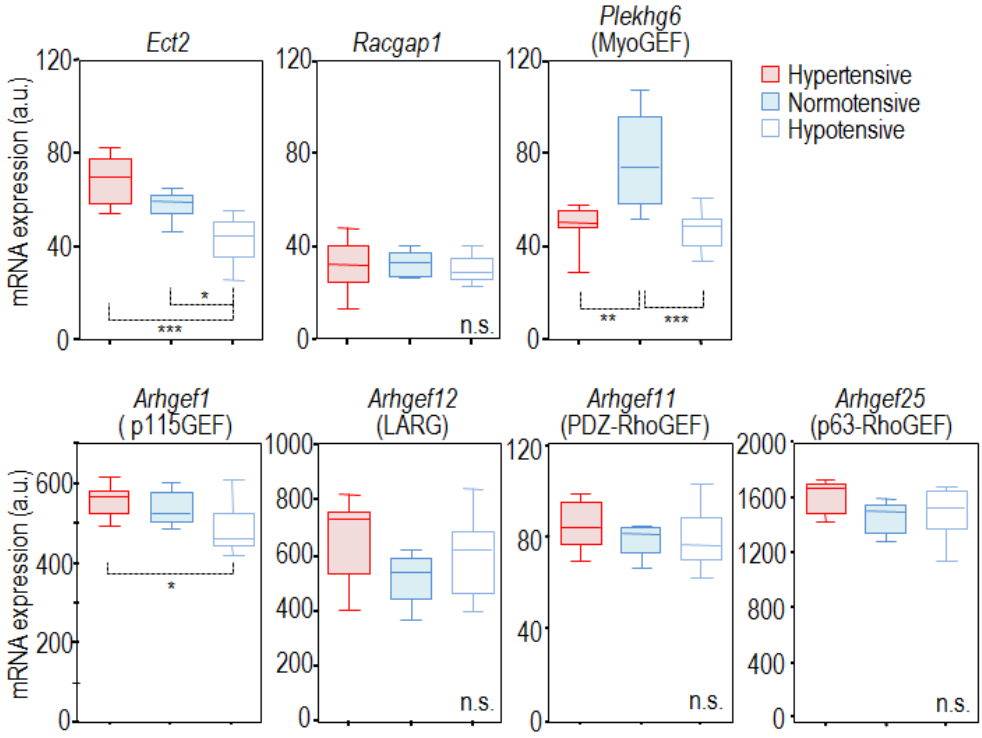

Supplementary Figure 6. Expression of RhoA regulators in murine aortas. Quantification of mRNA expression data for the indicated molecules from the GDS3672 GEO dataset. Data indicate mean ± SEM; *,p<0.05, **, p<0.01, ***, p<0.001; n.s., not significant. One-Way Anova test with Bonferroni's multiple comparison test.

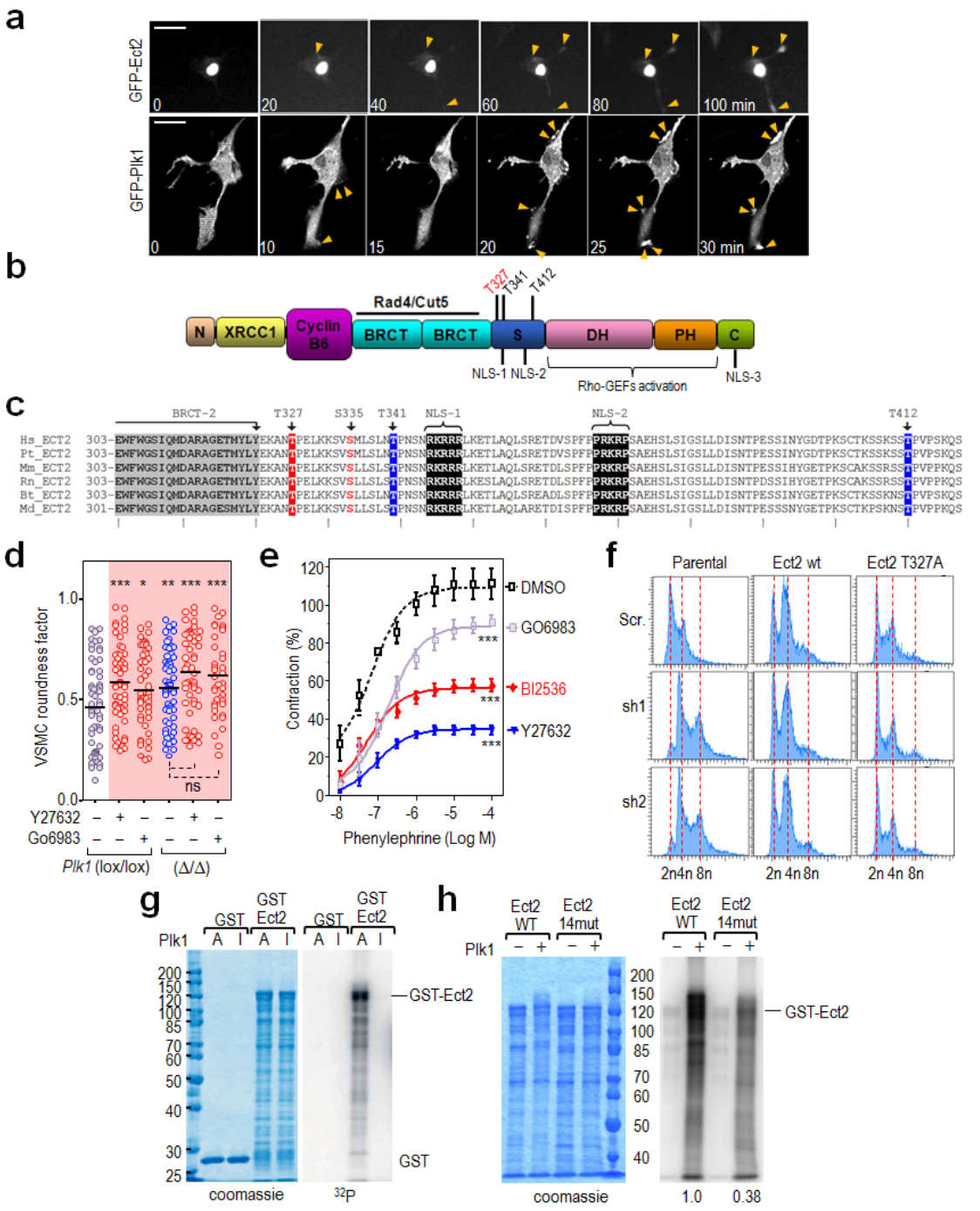

Supplementary Figure 7. Dynamical re-localization of Plk1 and Ect2 and analysis of Ect2 phospho-sites. (a) Time lapse microscopy images of cells expressing EGFP-Ect2 (upper panels) and EGFP-Plk1 (lower panels), after being stimulated with 2μM LPA. Cells are videorecorded each two minutes during at least 2 hours. Both Ect2 and Plk1 re-localized to the cell edge upon LPA addition (yellow arrowheads). (b) Ect2 protein cartoon showing the different domains and specific regions for nuclear localization (NLS), phosphorylation sites for Cdk1 (T341 and T412) and aPKC (T327), obtained from http://atlasgeneticsoncology.org/Genes/ECT2ID40400ch3q26.html. (c) Six different mammalian Ect2 sequences alignments at the "hinge" region showing the conservation of the phosphoresidues detected in our proteomic analysis (T327 and S335) as well as the conservation of the residues phosphorylated by Cdk1 (T341 and T412). Human (Hs, *Homo sapiens*); Chimpanzee (Pt, *Pan troglodytes*); Mouse (Mm, *Mus musculus*); Rat (Rn, *Rattus novergicus*); Cow (Bt, *Bos taurus*); Dolphin (Md, *Monodelphis domestica*). (d) Cell roundness in Plk1-null or control VSMCs untreated or treated either with 1 μM of the ROCK inhibitor

Y27632, or 1 μM of the PKC inhibitor Go6983. Mean ± SEM; n>50 cells per group in 3 different experiments. ns, not significant; *, p<0.05; **, p<0.01; ***, p<0.001; One-way ANOVA. (e) Ex-vivo aortic ring contraction analysis in the presence of increasing concentrations of phenylephrine and either DMSO as control (black line) or inhibitors of Plk1 (BI2536; red), ROCK (Y27632, blue) or PKC (Go6983, light purple). Contraction is expressed as a percentage of the maximal KCl-induced contraction normalized versus untreated samples. Data are mean ± SD; n=4 mice in each experimental group. ***, p<0.001; One-Way Anova. (f) Effects of the removal of Ect2 in the cell cycle. VSMCs were infected with two different lentiviral particles carrying a shRNA against the murine *Ect2* gene (sh1, Mm_Ect2_2126; sh2, Mm_Ect2_3164). Ect2 removal led to a severe change in ploidy due to lack of cytokinesis. These defects were partially rescued by expressing either a wild-type (wt) version of the human Ect2 cDNA, or the Ect2-T327A mutant. (g) Ect2 can be phosphorylated by Plk1 in vitro. In vitro kinase assays using Plk1-T210D constitutive active mutant (A) and Plk1-K82N as a kinase death mutant (I). Recombinant purified GST-Ect2 is used as a substrate for the kinase assays. Ect2 is phosphorylated when incubated with the active form of Plk1, whereas there is no signal of ^{32}P incorporation when the Plk1 kinase death is used. (h) Similar kinase assays were done using a GST-Ect2 mutated version, where the 14 putative sites for Plk1 phosphorylation were mutated to Alanine. Mutated residues are: Ser5, Ser20, Ser30, Thr255, Thr261, Ser294, Ser365, Ser378, Ser388, Ser394, Ser497, Ser525, Ser590, and Thr790. There is a reduction in Ect2 phosphorylation of about 60% in the mutant version when compared to the Ect2-WT protein. The fact that Ect2-14A mutant phosphorylation is not completely abolished suggests that Plk1 might still phosphorylate other Ect2 residues besides the canonical ones, at least in vitro.

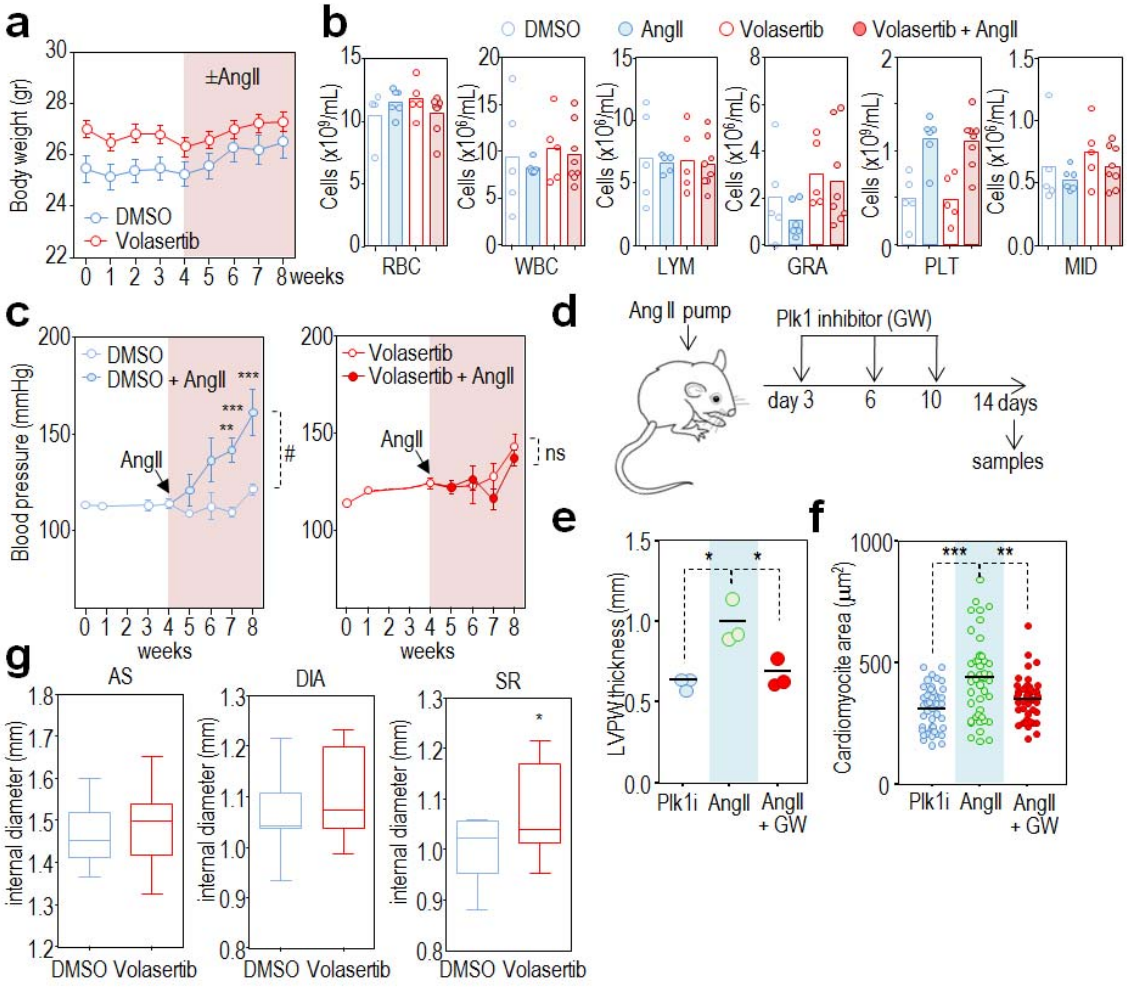

Supplementary Figure 8. Effect of Plk1 inhibitor volasertib in vascular structure and response to AngII. (a) Body weight of mice treated with volasertib (BI6727; red line; n=13 mice) or DMSO (blue line; 11 mice) during the 2 months duration of the experiment. At week 4 after starting the volasertib treatment, animals are stimulated with AngII osmotic pumps for 4 extra weeks. (b) Peripheral blood cell count in mice treated with volasertib and/or AngII. In (a) and (b) no significant differences were found between these cohorts of animals. Columns indicate mean; DMSO, n=5; AngII; n=6; Volasertib, n=5; Volasertib+AngII; n=8 mice. Student's t-test. (c) Effect of volasertib and AngII in blood pressure. Time 0 is the measurement immediate before volasertib treatment. Mice were infused with AngII as indicated by the arrow (week4). Volasertib injection resulted in an initial small increase in blood pressure [119.9 ± 2.2 mmHg in treated mice (n=13) versus 112.9 ± 1.8 mmHg in untreated mice (n=11)]. **, p<0.01; ***, p<0.001; Two-Way Anova. #, p<0.05; ns, not significant; Student's t-test. (d) Protocol for the concomitant treatment of mice with AngII and Plk1 inhibitor (GW843682X). (e) Histological quantification of the thickness of the left ventricle posterior wall (LVPW) in mice treated with AngII, GW843682X, or both (mean; n=3 mice per group). *, p<0.05; Student's t-test. (f) Cardiomyocyte area in in mice treated with AngII, Plk1 inhibitor, or both (mean; n=3 per mice group). **, p<0.01; ***, p<0.001; One-Way Anova. (g) Internal diameter of the ascendant (AS), diaphragmatic (DIA) and suprarenal (SR) aortic regions of mice treated during one month with volasertib (red boxes; n=13 mice) or solvent (blue boxes; n=11 mice), before AngII treatment. *, p<0.05; Student's t-test.

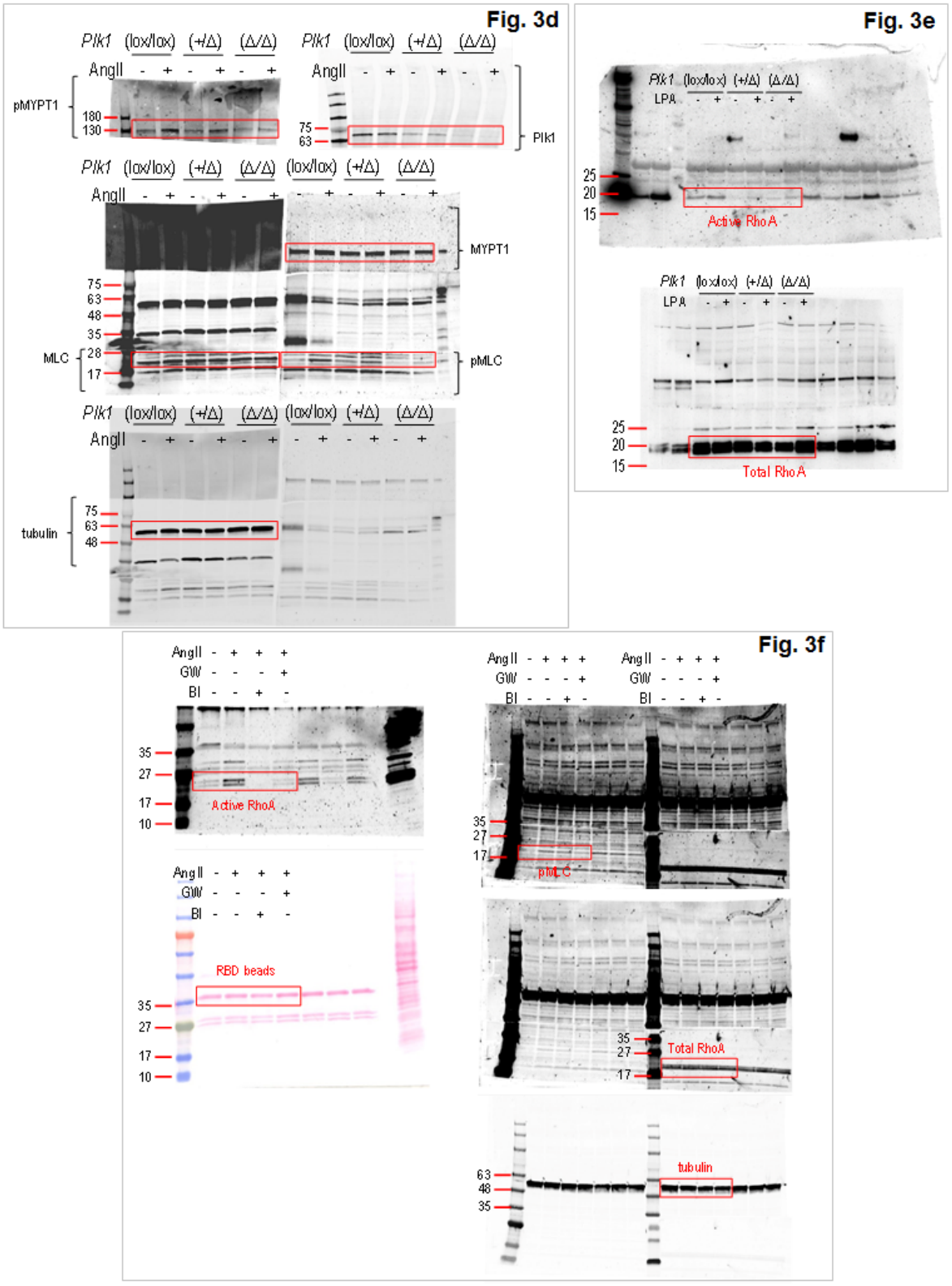

Supplementary Figure 9. Uncropped images for blots in Figure 3.

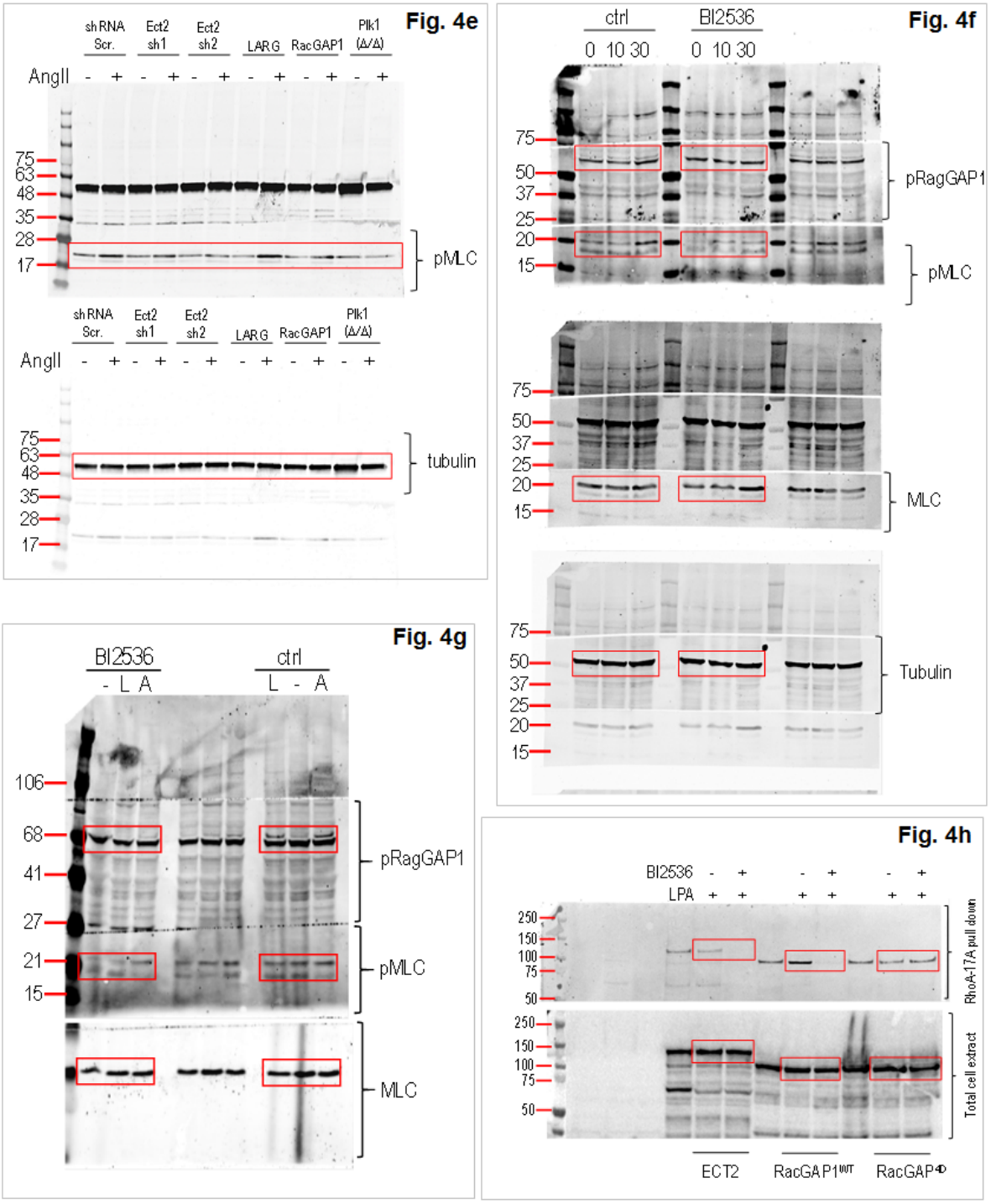

Supplementary Figure 10. Uncropped images for blots in Figure 4.

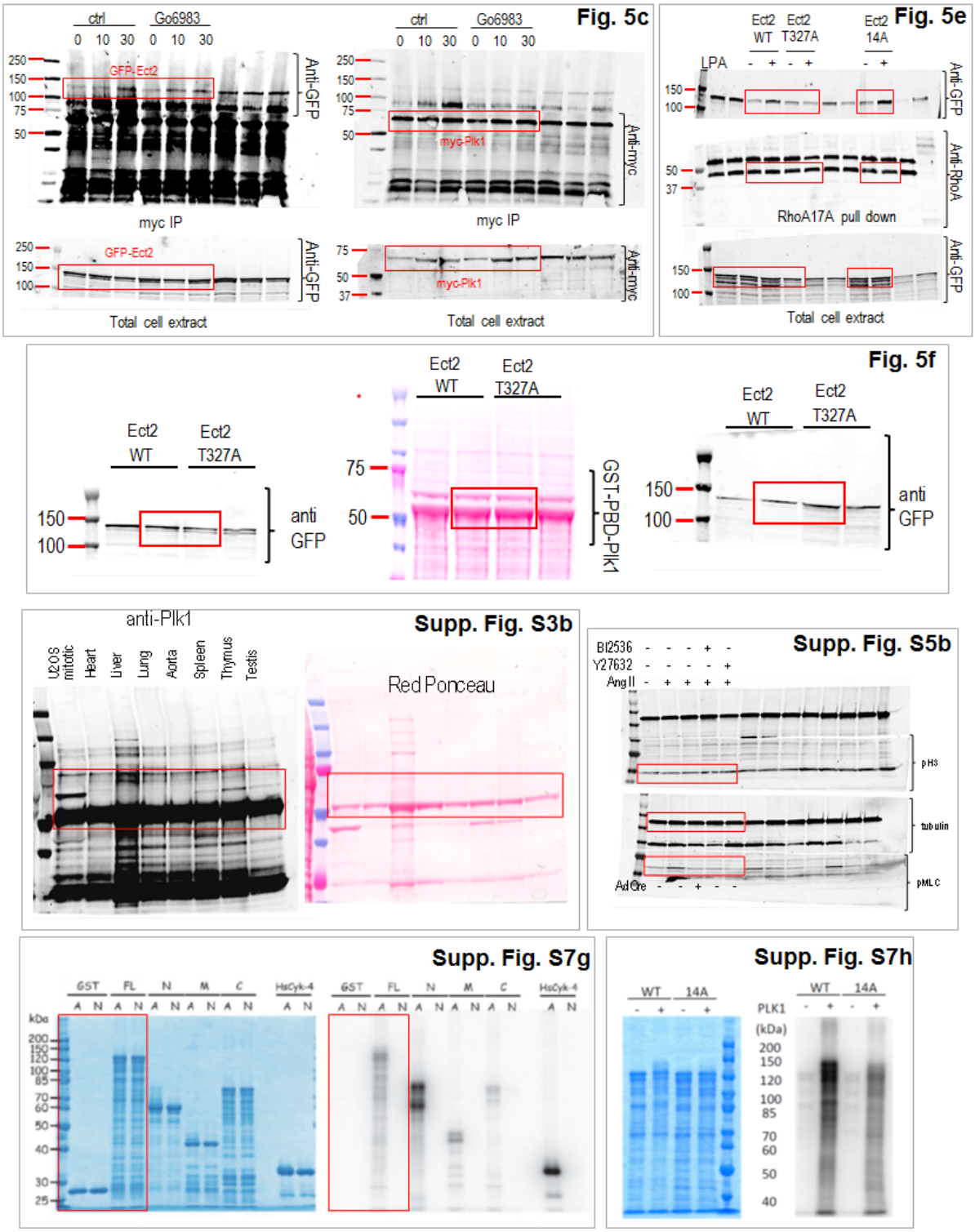

Supplementary Figure 11. Uncropped images for blots in Figures 5, S3, S5 and S7.

Supplementary Table 1. Non-tumoral pathologies observed in *Plk1* mutant mice

Pathology	*Plk1*(+/+) *N*=8	*Plk1*(+/–) *N*=11
Aorta wall dissection	0 (0%)	7(1*) (63.6%)
Myocardial recent/old infarcts	0 (0%)	3(1*) (27.3%)
Myointimal arterial hyperplasia	0 (0%)	3 (27.3%)
Granulomatous hepatitis	0 (0%)	4(1*) (36.4%)
Vascular congestion (liver, spleen, lungs, brain)	0 (0%)	6(1*) (54.5%)
Acute tubular necrosis (kidneys)	0 (0%)	1* (9.1%)
Hypertrofic right ventricle	0 (0%)	2 (18.2%)
Hypospermia	0 (0%)	3 (27.3%)
Increase in alveolar distal airspace caliber	0 (0%)	2 (18.2%)

* Females

Supplementary Table 2. Major biological functions deregulated in *Plk1*(+/–) aortas and genes differentially expressed in each category. (Fisher $p < 0.01$)

Category	*p*-value	Molecules
Skeletal and Muscular System Development and Function	6.7E-35-2.7E-02	CTGF, MYL6, TNNC1, MYLK2, TNNT2, ATP2A1, CXCL10, ALPK3, SMPX, TCAP, CASQ1, MGP, CASQ2, PLN, TNNC2, DCN, ITGA5, MYH7, FMOD, DES, MYL9 (includes EG:10398), PDLIM3, TRIM63, SMTNL1, ALDOA, MYBPC2, DTNA, CYR61, FHL1, BDNF, GPX1, TBX15, MYF6, RYR1 (includes EG:6261), MYH1, CKMT2, MYOM2, ACTN2, KBTBD10, MYOZ1, HRC, MYOCD, CNN1, TAGLN, MSTN, ITGB1BP3, PTGS2, TNNI1, CSRP3, FOXP2, MYL2, MYH11, SGCA, TBX18, MYOM1, TNNT3, NEB, POSTN, MYL4, CAV3, ITGB1BP2, ACTA1, ELN, SPP1, TNNI3, PGAM2, TRIM54, GSN, FOXC1, TTN, INHBA, BMPR1B, COL6A3, CAPN3, TPM1, MYH6, TNNT1, TNNI2, ACTA2 (includes EG:59), MYOT, COMP, TNFRSF12A, PHEX, SOX9, VGLL2, TGFB2, ACADM, PRDM6, PVALB, CXCR4, BGN, TRDN, TPM2, COL1A1, MYH2, CALD1, ACTN3, MYBPC3, LGALS1, TMOD4
Tissue Morphology	6.7E-35-2.7E-02	PLIN, MMP3, MYL2, ERAF, TNNC1, ATP2A1, TNNT2, MYLK2, MYH11, TBX21, SGCA, PTPRC, SMPX, MYOM1, TNNT3, CISH, CASQ1, MYL4, SERPINE1, ACTA1, CASQ2, ELN, ACACB, SPP1, TNNC2, DCN, PGAM2, TNNI3, TRIM54, MYH7, GSN, FOXC1, DES, INHBA, OTX2, TTN, MYL9 (includes EG:10398), BMPR1B, TRIM63, SMTNL1, RAG1, DTNA, MYBPC2, ALDOA, TPM1, MYH6, TNNT1, TNNI2, BDNF, GPX1, ACTA2 (includes EG:59), MYOT, SOX9, TGFB2, FABP4, RYR1 (includes EG:6261), MMP12, COL18A1, MYH1, CKMT2, MYOM2, CXCR4, BGN, ACTN2, KBTBD10, TRDN, VIM, TPM2, HRC, PRKAR2B, CNN1, MSTN, CALD1, TNNI1, PTGS2, ACTN3, TMOD4, MYBPC3
Tissue Development	2.22E-13-2.7E-02	PHLDA1, FOXP2, CTGF, MYL2, MYL6, TNNC1, TNNT2, MYLK2, ITGA8 (includes EG:8516), NME2, MYH11, SGCA, TBX18, NPNT, PTPRC, CXCL10, CYFIP2, ITGA9 (includes EG:3680), PPBP, POSTN, SERPINE1, CAV3, ITGB1BP2, EPHA7, ELN, NOX4, SPP1, PLN, NCAN, DCN, ITGA5, TNNI3, MYH7, GSN, ROR1, ANGPTL1, DES, FOXC1, INHBA, OTX2, TTN, BMPR1B, COL6A3, PDLIM3, CYR61, ITGB6, CAPN3, RBP4, ENAH, MYH6, SFRP2, ITGBL1, COL4A6, BDNF, ACTA2 (includes EG:59), GPX1, CXCR3, COMP, TNFRSF12A, SOX9, VGLL2, MYF6, TGFB2, PTPRZ1, COL18A1, HAS1, TMSB4X, SLC4A1, TNC, CXCR4, ACTN2, BGN, MYOZ1, RASGRP1, TAGLN, MSTN, PTGS2, TNNI1, CERCAM, CSRP3, MYBPC3
Cardiovascular Disease	3.95E-13-2.7E-02	CTGF, MYL2, MMP3, TNNC1, MYLK2, TNNT2, TBX21, SOD2, PDCD1, TCAP, POSTN, SERPINE1, CAV3, DSP, CASQ2, ACTA1, PTGIS, ELN, SPP1, PLN, ITGA5, TNNI3, TRIM54, MYH7, DES, TTN, BMPR1B, TRIM63, RAG1, DTNA, TPM1, MYH6, CRHR2, MB, MYH8, BDNF, GPX1, CXCR3, COMP, SOX9, TGFB2, FABP4, FABP3, MMP12, COL18A1, GABRA3, CXCR4, PDE5A, PTGS2, CSRP3, MYBPC3
Cardiovascular System Development and Function	2.93E-12-2.7E-02	ADAMTS8, CTGF, MYL2, TNNC1, TNNT2, MYLK2, MYH11, CXCL10, ALPK3, SOD2, PPBP, MGP, SERPINE1, CAV3, CASQ2, PTGIS, ELN, SPP1, PLN, DCN, ATP5A1, ITGA5, TNNI3, MYH7, ROR1, FOXC1, DES, ANGPTL1, INHBA, TTN, ATP5B, PDLIM3, CYCS (includes EG:54205), CYR61, TPM1, MYH6, CRHR2, MB, BDNF, GPX1, CXCR3, COMP, TNFRSF12A, SOX9, TGFB2, PTPRZ1, COL18A1, ACADM, TMSB4X, PVALB, CXCR4, VIM, HRC, COL1A1, SEMA3A, MYOCD, PTGS2, TNNI1, CSRP3, MYBPC3

Genetic Disorder	1.24E-11-2.7E-02	MCM6, ADAMTS8, TNNC1, TNNT2, ATP2A1, MYLK2, NDUFA1, ATP8B1, PTPRC, SOD2, TCAP, MGP, PTGIS, PLN, DCN, MYH7, DES, OTX2, DTNA, ALDOA, LDB3, CDKL5, FHL1, MYH8, BDNF, GAPDH, HADHB, MYF6, RYR1 (includes EG:6261), FXYD2, COL18A1, MMP17, PLOD2, ETFB, SLC4A1, PDE4DIP, VIM, BCL11A, SUCLG1, RASGRP1, MSTN, PTGS2, CSRP3, UQCRQ, CD247, FOXP2, MYL2, MMP3, ERAF, TBX21, SGCA, NEB, CAV3, ACTA1, DSP, ELN, H19, SPP1, TNNI3, GSN, FOXC1, TTN, COL4A5, BMPR1B, PYGM, COL6A3, CPT2, RAG1, CAPN3, HSPB3, TPM1, MYH6, TNNT1, COL4A6, CIITA, MYOT, COMP, PHEX, SOX9, SH2D1A, FLNA (includes EG:2316), ACADM, NDUFV1, UBB, SLC25A4, ETFA, CXCR4, BGN, LARS2, TPM2, HFE2, SERPINE2, COL1A1, MYH2, ACADVL, TPM3, PDE5A, CALD1, SDHD, LGALS1, MYBPC3
Skeletal and Muscular Disorders	1.92E-09-2.7E-02	MYH4, CTGF, MMP3, ATP2A1, SGCA, LDHB, CXCL10, PTPRC, SOD2, PDCD1, TCAP, NEB, MGP, SERPINE1, CAV3, DSP, ACTA1, SPP1, PDGFRL, TNNI3, TRIM54, MYH7, DES, INHBA, TTN, FAU, COL6A3, TRIM63, UQCRC2, DTNA, ALDOA, CAPN3, LDB3, TNNT1, FHL1, MYH8, BDNF, ACTA2 (includes EG:59), CIITA, MYOT, COMP, CHCHD2, PHEX, SOX9, SH2D1A, MYF6, FLNA (includes EG:2316), FABP4, RYR1 (includes EG:6261), GABRA3, MYH1, UBB, CXCR4, BGN, VIM, TPM2, COL1A1, HP, MYH2, TPM3, CALD1, MSTN, PTGS2, LGALS1
Cancer	1.26E-08-2.7E-02	MYH4, CTGF, ATP2A1, GPSM2, ATP8B1, COX6A2, PTPRC, CXCL10, ALPK3, SOD2, ITGA9 (includes EG:3680), ASB5, MGP, SERPINE1, PTGIS, CSRP2, TNNC2, DCN, RPL27, ITGA5, OTX2, MYL9 (includes EG:10398), PDLIM3, CYCS (includes EG:54205), ALDOA, DTNA, CYR61, ITGB6, LDHA, FTH1, ITGBL1, BDNF, MYH8, GPX1, CXCR3, CD52, MYF6, FABP4, FABP3, COL18A1, HAS1, GABRA3, TMSB4X, MYH1, PLOD2, TNC, DBI, OBSCN (includes EG:84033), VIM, MLF1, SEMA3A, HP, NOV, BCL11A, RASGRP1, CNN1, TAGLN, MSTN, PTGS2, CSRP3, CD247, CFD, MMP3, NME2, MRVI1, PAX5, TNNT3, POSTN, SPP1, H19, RRAD, PDGFRL, TNNI3, HHIP, GSN, FOXC1, ANGPTL1, INHBA, RASD1, BMPR1B, COL6A3, TES, RAG1, RBP4, CAPN3, TPM1, SDHB, SFRP2, COL4A6, TNNI2, ACTA2 (includes EG:59), SLC25A5, TNFRSF12A, IL17B, SOX9, HINT1 (includes EG:3094), FLNA (includes EG:2316), RPS16, TGFB2, PTPRZ1, MMP12, CKM, ETFA, CXCR4, BGN, NDUFA13, TPT1 (includes EG:7178), COL1A1, MYH2, PRKAR2B, MYOZ2, COX5A, PDE5A, CALD1, SDHD, WISP1, ACTN3, LGALS1
Energy Production	2.07E-08-4.45E-05	MYH6, COX17, ATP5O, SLC25A4, COX6A1, UQCR, ATP5A1, COX6C, COX8A, MYH7, COX7A1, COX6A2, ATP5C1, ATP5B, ATP5E, ATP5J2, ATP5F1, COX4I1
Nucleic Acid Metabolism	2.07E-08-2.7E-02	ATP5C1, MYH6, ATP5O, ATP5B, ATP5E, ATP5A1, ATP5J2, PDE5A, MYH7, ATP5F1
Small Molecule Biochemistry	2.07E-08-2.7E-02	MYH6, PLIN, BDNF, RAB27B, GPX1, ANKRD23, PTPRC, HADHB, ADFP, PPBP, ATP5J2, FABP4, GPX4, FABP3, ATP5F1, ACADM, HAS1, CKMT2, PTGIS, SPP1, ACACB, ATP5O, CKM, ATP5A1, MYH7, GSN, ATP5C1, CIDEA, ATP5B, ACADVL, ATP5E, CPT2, CYCS (includes EG:54205), PDE5A, PTGS2, LGALS1

Supplementary Table 3. Canonical cellular pathways deregulated in *Plk1*(+/–) aortas and genes differentially expressed in each category. (Fisher 0.01)

Pathway	-Log (*p*-value)	Ratio	Molecules
Oxidative Phosphorylation	2.49E01	2.29E-01	NDUFA4, SDHB, COX6A1, UQCR, COX8A, COX5B, NDUFB8, NDUFA1, COX6A2, NDUFB10 (includes EG:4716), UQCRH, NDUFB9, ATP5H (includes EG:10476), ATP5J2, UQCRFS1, NDUFB6, ATP5F1, COX4I1, NDUFV1, COX17, ATP5O, ATP5A1, COX6C, COX7A1, NDUFA13, ATP5C1, NDUFS5, NDUFB11, ATP5B, ATP5E, UQCRC2, COX5A, SDHD, CYC1, UQCRC1, UQCRQ
Mitochondrial Dysfunction	2.03E01	1.82E-01	NDUFA4, SDHB, COX6A1, COX8A, COX5B, NDUFB8, NDUFB10 (includes EG:4716), COX6A2, UQCRH, NDUFB9, SOD2, NDUFB6, UQCRFS1, GPX4, COX4I1, NDUFV1, COX17, ATP5A1, COX6C, COX7A1, NDUFA13, ATP5C1, NDUFS5, NDUFB11, ATP5B, UQCRC2, COX5A, SDHD, CYCS (includes EG:54205), CYC1, UQCRC1
Calcium Signaling	1.69E01	1.53E-01	MYH4, TPM1, MYH6, TNNT1, MYL6, TNNI2, MYL2, MYH8, TNNC1, ATP2A1, ACTA2 (includes EG:59), TNNT2, MYH11, TNNT3, CASQ1, RYR1 (includes EG:6261), MYL4, ACTA1, CASQ2, MYH1, TNNC2, TRDN, TPM2, TNNI3, MYH7, MYL7, MYL9 (includes EG:10398), MYH2, PRKAR2B, TPM3, TNNI1
Actin Cytoskeleton Signaling	7.67E00	9.91E-02	MYH4, MYH6, MYL2, MYL6, MYH8, ACTN2, MYLK2, ACTA2 (includes EG:59), ITGA5, MYH11, MYH7, GSN, TTN, MYL7, MYL9 (includes EG:10398), CYFIP2, MYH2, MYL4, ACTA1, ACTN3, TMSB4X, MYH1
Hepatic Fibrosis / Hepatic Stellate Cell Activation	6.63E00	1.19E-01	MYH4, MYH6, CTGF, MYL2, MYL6, MYH8, ACTA2 (includes EG:59), MYH11, MYH7, MYL7, MYL9 (includes EG:10398), COL1A1, MYH2, TGFB2, MYL4, MYH1
Ubiquinone Biosynthesis	5.53E00	9.62E-02	NDUFA4, NDUFV1, NDUFB9, NDUFS5, NDUFB11, NDUFB6, NDUFB8, NDUFA1, NDUFA13, NDUFB10 (includes EG:4716)
Tight Junction Signaling	5.43E00	9.76E-02	MYH4, MYH6, MYL2, MYL6, MYH8, ACTA2 (includes EG:59), MYH11, MYH7, MYL7, MYL9 (includes EG:10398), PRKAR2B, MYH2, TGFB2, MYL4, ACTA1, MYH1
Propanoate Metabolism	2.96E00	5.56E-02	HADHB, ACACB, ACADVL, SUCLG1, ACADM, LDHB, LDHA
Citrate Cycle	2.94E00	8.47E-02	SDHB, IDH3G, SUCLG1, SDHD, MDH2
Integrin Signaling	2.69E00	6.74E-02	MYL2, ACTN2, ITGA8 (includes EG:8516), ACTA2 (includes EG:59), MYLK2, ITGA5, TTN, MYL7, ITGA9 (includes EG:3680), ITGB6, ACTN3, ACTA1, CAPN3
Glycolysis/Gluconeogenesis	2.42E00	5.67E-02	ENO3, PGAM1, GAPDH, PGAM2, ALDOA, PDHB, LDHB, LDHA
Caveolar-mediated Endocytosis	2.33E00	8.64E-02	ITGA9 (includes EG:3680), FLNA (includes EG:2316), ACTA2 (includes EG:59), ITGA8 (includes EG:8516), ITGA5, ITGB6, ACTA1
Regulation of Actin-based Motility by Rho	2.15E00	7.61E-02	MYL6, MYL2, ACTA2 (includes EG:59), MYL4, GSN, ACTA1, MYL7

Supplementary Table 4. Oligonucleotides used for quantitative RT-PCR.

Oligo name	Sequence
Mm_Plk1_FW	5'- CCTATTACCTGCCTCACCAT -3'
Mm_Plk1_RW	5'- CAATGGCCTCATTTGTCTCC -3'
Mm_Ect2_FW	5'- TGCCGCAGGTTGAAGCAAGAGT -3'
Mm_Ect2_RW	5'- AACGGCAAGGGCTCTCCCCT -3'
Mm_RacGAP1_FW	5'- TGGACCAGGAGTCGCGGGAA -3'
Mm_RacGAP1_RW	5'- GTCGGCCAGCATGCCCTCTC -3'
Mm_MyoGEF_FW	5'- TGGAGTGGACCCTAGTCGCCG -3'
Mm_MyoGEF_RW	5'- CTGGTGGCAAAGCTGGCGGT -3'
Mm_p115_FW	5'- GGTCGAGGCTGATGAGAAGCCAG -3'
Mm_p115_RW	5'- CTCAGGGGTGGCTCGTCGGG -3'
Mm_LARG_FW	5'- GGTCTTGTTCAGCGCTGTGTGAT -3'
Mm_LARG_RW	5'- CTCCCCCACGAGCACAGGACT -3'
Mm_Gapdh_FW	5'- GCCACCCAGAAGACTGTGGATGGC -3'
Mm_Gapdh_RW	5'- CATGATGGCCATGAGGTCCACCAC -3'